

*Chapter 1***Electronic transport and localization in short and long DNA****H. Wang, R. Marsh, J. P. Lewis,^a R. A. Römer^b ***^aDepartment of Physics and Astronomy, Brigham Young University, Provo, UT 84602-4658, U.S.A.^bDepartment of Physics and Centre for Scientific Computing, University of Warwick, Coventry CV4 7AL, United Kingdom

The question of whether DNA conducts electric charges is intriguing to physicists and biologists alike. The suggestion that electron transfer/transport in DNA might be biologically important has triggered a series of experimental and theoretical investigations. Here, we review recent theoretical progress by concentrating on quantum-chemical, molecular dynamics-based approaches to short DNA strands and physics-motivated tight-binding transport studies of long or even complete DNA sequences. In both cases, we observe small, but significant differences between specific DNA sequences such as periodic repetitions and aperiodic sequences of AT bases, λ -DNA, centromeric DNA, promoter sequences as well as random-ATGC DNA. (*Revision* : 1.15)

1. Introduction

Charge transfer in DNA is currently the subject of intense theoretical and experimental investigations [1–4]. DNA, which is the blueprint of life, is being considered as a molecular wire in a new generation of electronic devices and computers. However its electronic properties are elusive and remain controversial. Despite the current debate, the subject is far from new. Soon after Watson and Crick discovered the double-helix structure of DNA [5], Eley and Spivey were the first to suggest that DNA could serve as an electronic conductor [6]. The notion of a molecular wire is thought to apply to the DNA double helix because of its π -electron (the π -way) system of bases stacked upon each other. More recently, Barton and colleagues [7] measured the fluorescence of an excited molecule and found that it no longer emitted light when attached to DNA.

*Work partially supported by the Royal Society.

Their results suggested that this “fluorescence quenching” was due to the charge on the excited donor molecule leaking along the length of the DNA to a nearby acceptor molecule.

Other extensive experimental and theoretical work over the past decade has led to substantial clarification of charge-transfer mechanisms in DNA [7–20]. The dominant mechanisms appear to be both short-range quantum mechanical tunneling and long-range thermally activated hopping. Guanine has the highest occupied molecular orbital (HOMO) level of the four bases, and can act as a trap for holes. Experiments on repeats of this base are used to investigate long range hopping, and models have been developed to clarify the long range hopping data in G-repeats [14]. Charge transport in DNA is also made more complex because of the influences of the local environment, such as counterions, thermal vibrations, contact resistance, and sequence variability, which are difficult to control [21–25]. The charge-transfer mechanisms in DNA and/or whether DNA is a good conductor or not remains somewhat unsettled. Indeed, theory is of great help in understanding these phenomena, but given the computational cost of full-scale calculations on the realistic DNA systems, theoretical efforts to date have mostly been limited to small- and medium-size model systems [26–28], to dry DNA molecules [23, 29, 30], or to larger systems using model Hamiltonians [31–42] and semi-empirical studies [22, 43–53].

In this review, we shall first focus on the use of quantum-chemical methods which can treat smaller, but atomistically correct segments of DNA in Sec. 2. After an introduction to the construction of the DNA molecules and the density-functional based methods in Sec. 2.1 - 2.3, we then present results, many of which are new, in sections 2.4 to 2.5. In the next large section 3, we use the lessons learned from the atomistic approach and now study an effective and necessarily rather coarse-grained Hamiltonian model of DNA to reveal the interplay of sequence fidelity and transport. Again, models, methods and DNA sequences are introduced in Sec. 3.1 - 3.3. Sections 3.4 and 3.5 include the obtained results. We conclude and summarise in Sec. 4.

2. Quantum chemical methods for *short* DNA strands

Within a density functional based local orbital tight-binding-like formalism, more complex problems can be investigated with a modest decrease in the accuracy. This is particularly useful where a quantum mechanical description is important to the investigated system’s fundamental chemistry, yet where a smaller model system would inadequately describe the proper physical environment. With the increase in computational power, great effort has been made by the electronic-structure community to optimise the performance of quantum

mechanical methods. Calculating larger systems without making stringent approximations has only been possible within the past few years. In this chapter, we theoretically investigate the electronic states of model DNA structures as the molecule undergoes classical thermal motion at room temperature by means of marrying classical molecular dynamics simulations with an electronic structure density-functional method. We investigate the dynamics of the DNA structure and its impact on the electronic structure. A similar approach was recently used to postulate the charge migration mechanism in DNA, with injected charges being gated in a concerted manner by thermal motions of hydrated counterions [17]. Here we study a longer oligonucleotide duplex than previous studies, and demonstrate with the complete system that its electronic states dynamically localize. The mechanism is an Anderson *off-diagonal* dynamic disorder model similar to the static disorder that leads to localised band-tail states in amorphous semiconductors [54–57]. The concept of static Anderson localization in DNA has previously been considered by Ladik [58, 59]. We show that localization in DNA reaches far deeper in energy than just band tail states. We demonstrate for the first time this effect in a hydrated poly(dA)-poly(dT) 10 base-pair fragment; this represents one complete turn of the B-DNA double helix.

2.1. Generating the poly(dA)-poly(dT) DNA structures

In this chapter, we consider thermal fluctuations of a poly(dA)-poly(dT) DNA 10-mer duplex fragment at room temperature from classical MD simulations; therefore, aperiodic structures of DNA are generated throughout the simulation. With our local-orbital density-functional method, we compare the electronic states of an idealised model periodic canonical B-DNA poly(dA)-poly(dT) DNA structure with those thermally-distorted aperiodic poly(dA)-poly(dT) DNA structures generated from the MD simulation.

Canonical B-DNA 10-base pair models of poly(dA)-poly(dT) were built into a Arnott B-DNA [60] model using the nucgen DNA builder contained within AMBER 5.0 [61]. Classical molecular dynamics trajectories of the B-DNA models, including explicit water and sodium counterions, were generated using the CHARMM (version c26n1) [62]. Both models were solvated with enough pre-equilibrated TIPSP [62] water to add 12.0 Å to the maximal distance extent of the DNA. Net-neutralising Na⁺ ions [63] were placed off the phosphate oxygen bisector and then minimised (with larger, 5.0 Å, van der Waals radii) *in vacuo* prior to solvating the system. Equilibration involved the application of harmonic positional restraints (25.0 kcal/mol²) and 250 steps of ABNR minimisation, followed by 25 ps of MD where the temperature was ramped up from 50 to 300 K in 1 ps intervals. The initial equilibration was performed with the Cornell et al. force field [64]. Subsequent equilibration with the ??? (BMS)

force field of Langley [65], involved 250 steps of ABNR minimisation followed by 5 ps of MD with position restraints.

All production simulations were performed without any restraints and the BMS force field of Langley. Production simulation was performed for 10 nanoseconds with CHARMM (version c26n1) [62] in a consistent manner. This involved constant temperature (300 K, mass = 1000) [66] and pressure (1 atm, piston mass = 500 amu, relaxation time = 20 ps⁻¹) [67], 2 fs time steps with the application of SHAKE [68] on hydrogen atoms, accurate use of the particle mesh Ewald method [69] (~1.0 grid size with 6th order B-spline interpolation and a Ewald coefficient of 0.34) in rhombic dodecahedral unit cells ($x = y = z$, $\alpha = 60^\circ$, $\beta = 90^\circ$, $\gamma = 60^\circ$), a heuristically updated atom based pairlist built to 12.0 Å and cutoff at 10.0 Å with a smooth shift of the van der Waals energies. These methods have proven reliable for representing DNA duplex structure [70, 71] and the BMS force field very accurately models B-DNA crystal structures [65, 72].

After an initial equilibration of an explicitly solvated 10-mer B-DNA poly(dA)-poly(dT) with explicit Na⁺ ions, production molecular dynamics simulations (applying an accurate particle mesh Ewald treatment of the electrostatics) were performed for 10 ns. As shown in Fig. 1, a plot of the all-atom root-mean-squared deviation over the entire run is rather stable, and although thermal fluctuations are clearly evident, no large scale distortions of the structure were observed (beyond sugar repuckering, and expected base and backbone fluctuations).

2.2. Electronic structure calculations of molecular dynamics snapshots

A stable portion of the trajectory from 1.5-2.5 ns, at 0.5 ps intervals, was analysed further using the FIREBALL DFT methodology [73]. FIREBALL is a first principles tight-binding molecular dynamics (TBMD) simulation technique based on a self-consistent version of the Harris-Foulkes [74, 75] functional [76]. In this method, confined atomic-like orbitals are used as a basis set for the determination of the occupied eigenvalues and eigenvectors of the one-electron Hamiltonian. The “fireball” orbitals, introduced by Sankey and Niklewski [77], are obtained by solving the atomic problem with the boundary condition that the atomic orbitals vanish outside and at a predetermined radius r_c where wavefunctions are set to be zero. This boundary condition is equivalent to an “atom in the box” and has the effect of raising the electronic energy levels due to confinement. An important advantage of the Sankey and Niklewski basis set is that the Hamiltonian and the overlap matrix elements of the system are quite sparse for large systems, reducing overall computation time. A summary of the method is given in Ref. [73] and references therein. All poly(dA)-poly(dT)

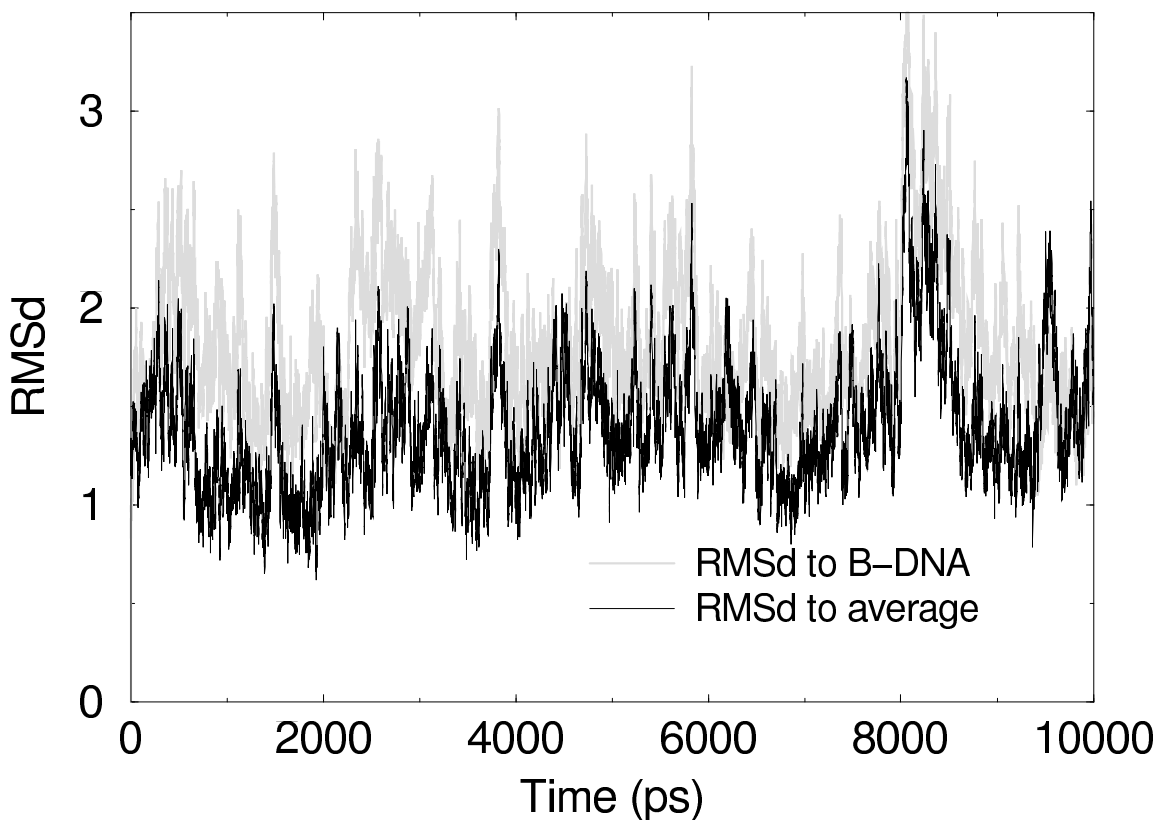


Fig. 1. Shown in black and gray are the all-atom best-fit root-mean-squared deviations (in Å) as a function of time compared to canonical B-DNA (gray) and the straight coordinate average structure from the 1.5-2.5 ns portion of the trajectory (at 0.5 ps intervals).

DNA atoms, including phosphate groups and backbone atoms are included in the single-point calculations which contained 10 base pairs (644 atoms). Although the MD simulations are performed with full hydration and counterions, we include only 350 water molecules in our electronic structure calculations; this number of molecules represents approximately 2 solvation layers surrounding the molecule. Adding all water and cation atoms to more correctly represent the environment surrounding the DNA molecule will be the subject of future work.

2.3. Quantifying the Degree of Localization

The phenomena of Anderson localization [54, 78] refers to the localization of mobile quantum mechanical entities, such as spin or electrons, due to impurities, spin diffusion, or randomness. Anderson localization applied to DNA may come from two distinct mechanisms, *diagonal* or *off-diagonal* disorder. *Diagonal* disorder induced localization occurs from variations of the sequence

along the base stack, and *off-diagonal* disorder occurs by variations either from bonding between bases along the stack or from hydrogen bonding variations across the double helix. The qualitative physics of localization is described by an Anderson model [54],

$$H = \sum_i \epsilon_i c_i^\dagger c_i + \sum_{i,j} t_{i,j} c_i^\dagger c_j + t_{j,i} c_j^\dagger c_i, \quad (1)$$

where each molecular orbital (MO) i of a base has energy ϵ_i and interacts with its nearest neighbour base MO j ($i \neq j$) with a Hamiltonian hopping interaction of t_{ij} . The Anderson model of *diagonal* disorder randomly varies the on-site Hamiltonian matrix elements (diagonal) ϵ_i [78] and describes the A-T-G-C random sequencing of DNA [31].

Here we focus on B-DNA structures of poly(dA)-poly(dT) in which there exists only one base pair combination A-T; each strand has only a single type of base in its stack. In this system, only *off-diagonal* disorder [79] may occur. The bonds within a single base are strong, but thermal fluctuations coupled with weak π -bonding occurs along the stack and the weak hydrogen bonds across the strands of the DNA double helix allows individual bases significant freedom of movement, including transient base pair opening and DNA breathing events over millisecond time scales [80] and large fluctuations in the structure [81]. Stochastic fluctuations of the weak bonding modulates the electronic coupling, t_{ij} , between adjacent bases. If the dynamic fluctuations of t_{ij} are large enough, localised electronic states are produced as in an amorphous solid.

We quantify the spatial extent of an electronic state by defining the number of accessible atoms, W , from the electronic state quantum *entropy*. From a particular state ν , the wavefunction $\psi(\nu)$ has a Mulliken population $p_i(\nu)$ on atom i , which loosely is considered the probability that an electron in state ν and resides on a particular atom i . The populations are normalised, $\sum_i p_i(\nu) = 1$. From probability theory, we define a quantum entropy for state ν as,

$$S(\nu) = - \sum_i p_i(\nu) \ln p_i(\nu).$$

For example, a state ν with equal probabilities over N_0 atoms ($N_0 \leq N_{Total}$), gives an entropy of $\ln N_0$. From Boltzmann's equation, we can determine the number of accessible atoms $W(\nu)$ for electronic state ν as $S(\nu) = \ln W(\nu)$, or $W(\nu) = e^{S(\nu)}$.

Our example state with equal probabilities spread over N_0 atoms gives the expected result, $W(\nu) = N_0$. For the complex electronic states of DNA, the number of accessible atoms $W(\nu)$ gives a quantitative, and easily calculable, measure for how many atoms a particular electronic state $\psi(\nu)$ reaches.

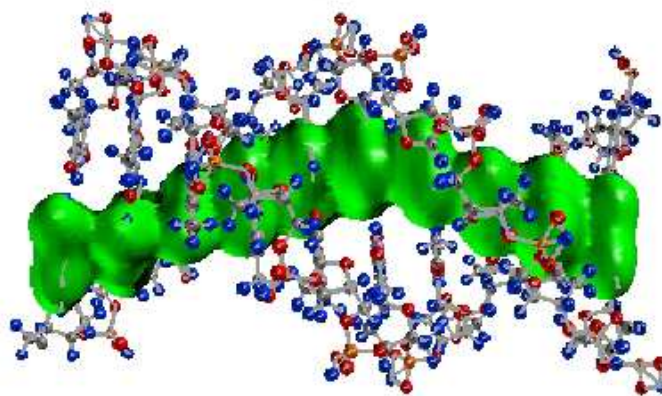
2.4. Electronic states of a periodic poly(dA)-poly(dT) DNA

To demonstrate that localization is not due to limitations of using localized orbitals, a 10-base pair periodic structure of poly(dA)-poly(dT) was created based on the Arnott B-DNA [60] fiber model. Each base pair is rotated by 36° and translated by 3.38 Å; therefore, 10 base pairs complete one full pitch of the double helix and periodicity is enforced in the program. The population densities for the highest occupied molecular orbital (HOMO) and the lowest unoccupied molecular orbital (LUMO) are plotted in Fig. 2. As seen from this figure, both the HOMO and LUMO states exhibit very extended and periodic (Bloch-like) states throughout the molecule. No localization is evident.

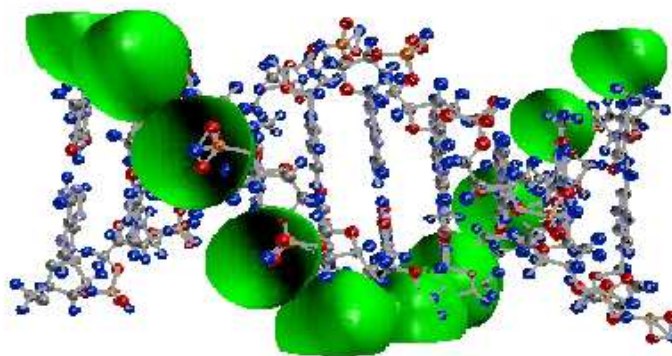
2.5. Electronic states of sampled poly(dA)-poly(dT) DNA configurations

We now consider results for a single configuration from the MD simulation (labeled step 3001, the first coordinate set 0.5 ps after a 1.5 ns production simulation). Figure 3 shows the number of accessible atoms, $W(\nu)$, for each electronic state at this time step for the dehydrated structure. The $W(\nu)$ for the hydrated DNA structure is shown in Fig. 4. For both structures it is important to note that, near the HOMO and LUMO, the number of accessible atoms is quite small (< 30), demonstrating a large degree of localization for the wavefunctions. This localization extends over several eV and is deeper than just the band tail states. States further away from the HOMO and LUMO become considerably delocalised and the number of accessible atoms is much larger. The number of accessible atoms is also small for the lowest energy levels; these deep states consist mainly of 2s levels of oxygen and nitrogen atoms. For the hydrated DNA molecule, the localized states near the HOMO are mainly due to the surrounding water molecules. Just below these water-related localized electronic states are the localized electronic states residing on the DNA bases. This may account for the smaller band gap of the hydrated structure compared with the electronic structure of the dehydrated DNA. Overall, the electronic structures for both the hydrated and dehydrated DNA molecules show remarkable similarities. These results imply that the aquatic environment does not significantly alter DNA's electronic structure. Therefore, we focus our studies on the electronic structures of dehydrated DNA molecules.

The degree of localization for two example band states (1074 and 614 - larger number implies higher eigenvalue) in the dehydrated DNA structures can be seen in Fig. 5 where population density plots of a localised and delocalised state are shown. As more configurations are analysed, we see consistently that the number of accessible atoms for the energy levels near the HOMO primarily consist of around 20 atoms. However, as a function of time, different sets of atoms are involved. To determine where the localization occurs, we compute



HOMO



LUMO

Fig. 2. Population densities for the highest occupied molecular orbital (HOMO) and the lowest unoccupied molecular orbital (LUMO) are shown for periodic poly(dA)-poly(dT) DNA (10 base pairs). Both molecular orbitals exhibit very extended and periodic (Bloch-like) states throughout the molecule.

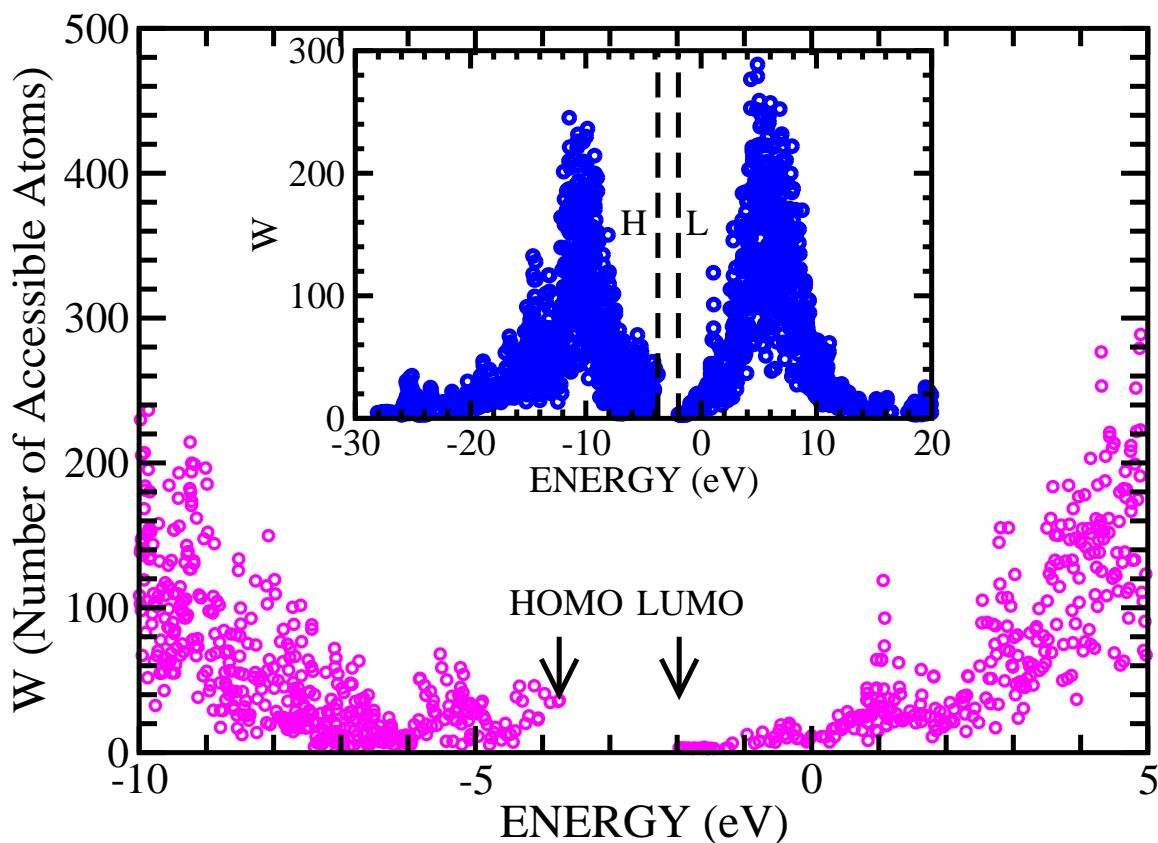


Fig. 3. Number of accessible atoms, $W(\nu)$, for each electronic state near the HOMO and LUMO levels. Inset shows number of accessible atoms for all levels. The system contains 10 basepairs of DNA (644 atoms).

a residence of each state according to the specific DNA component - adenine base, thymine base, ribose backbone, or phosphate group and determine where the high probability regions are located. Further investigation indicates the residence localization for the highly localised states near the HOMO are contained approximately on single bases in the DNA molecule; adenine for states very near the HOMO and thymine for states slightly lower in energy. This regional population information for the HOMO on adenine is plotted in Fig. 6. The more extended states (~ 8 eV to ~ 18 eV below the HOMO) are found to reside throughout the various DNA components.

As the simulation proceeds in time, the residence of the HOMO level moves from base to base along the poly(dA)-poly(dT) system and large jumps in sequence are possible over this 0.5 ps resolution time scale. This fluctuating residency of the HOMO is visualised in Fig. 7, which shows population density plots for a series of snapshots at different times ($t=3001, 3004, 3007, \text{ and } 3010$).

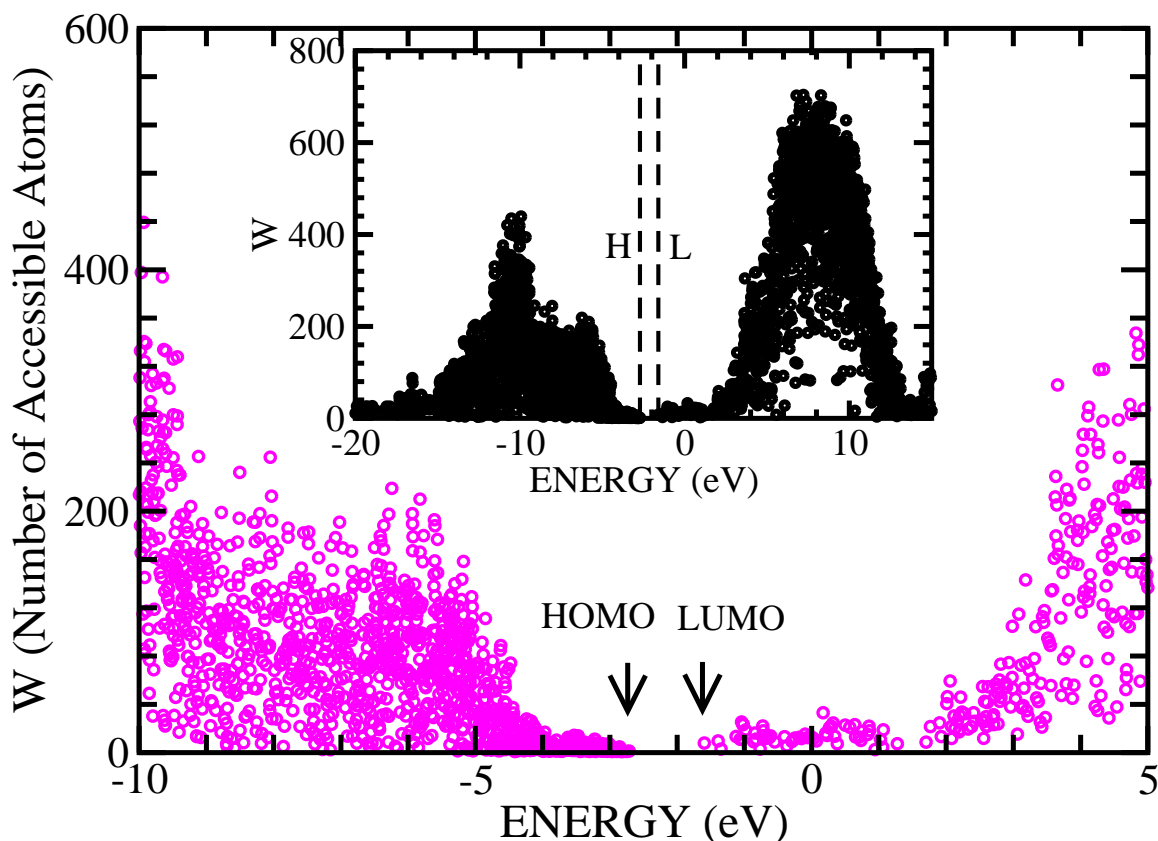
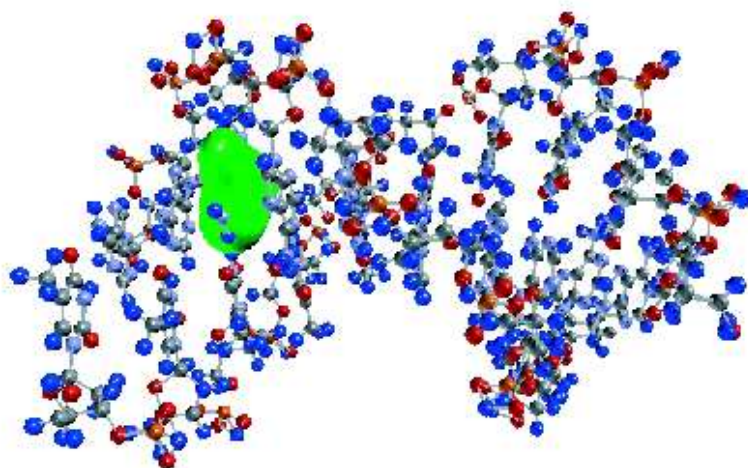


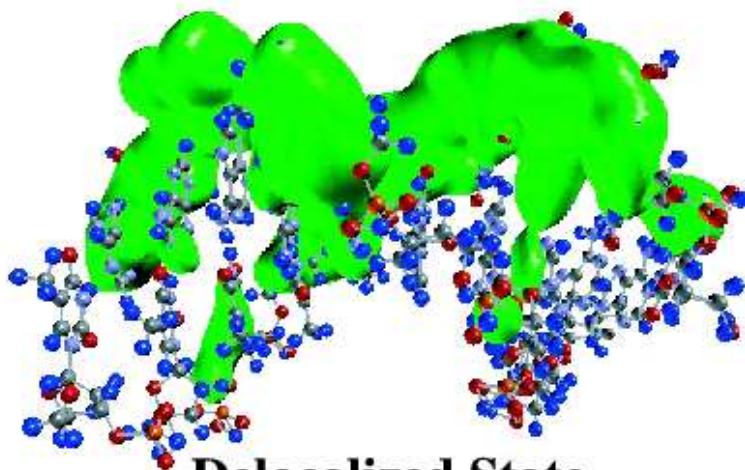
Fig. 4. Number of accessible atoms, $W(\nu)$, for each electronic state near the HOMO and LUMO levels. Inset shows number of accessible atoms for all levels. The system contains 10 basepairs of DNA (644 atoms) and 350 water molecules.

The separation between these snapshots is 1.5 ps. Figure 8 shows the location of the HOMO for all 100 snapshots where the electronic structure was calculated in this work. The population is localised on different adenine bases as time progresses and appears to chaotically oscillate between one end of the DNA molecule to the other. The HOMO level's localization on one adenine base is traded for localization on another adenine base through the dynamical simulation. Physically, this trading ought to reflect concerted fluctuations assignable to off-diagonal dynamical disorder in a regular homooligonucleotide duplex. Based on these results, it is conceivable that electron (hole) transfer will occur as two or more localised MO levels are dynamically trading places. Moreover, this swapping may be gated by thermal fluctuations of hydrated counterions, in accordance with the ion-gating transport mechanism proposed in Ref. [17].

Finally, it is of considerable interest to compare our above results to the known literature data on this theme. Specifically, our findings are in parallel



Localized State
($t=3001$, band=1074, $W=10.2$)



Delocalized State
($t=3001$, band=614, $W=225.5$)

Fig. 5. Example of a localised and a delocalised state for two different states in poly(dA)-poly(dT) at time step 3001. For reference, the HOMO is band 1094.

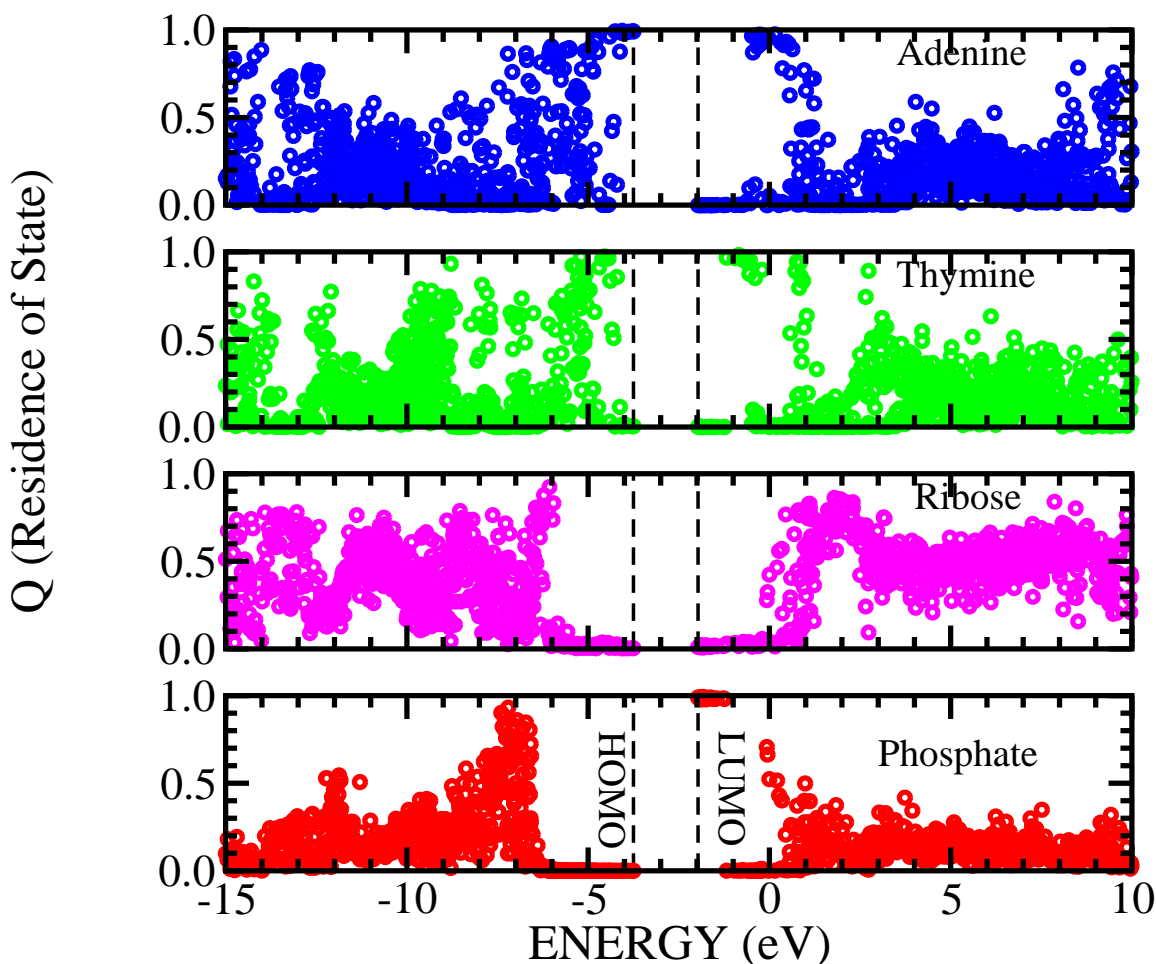


Fig. 6. Residence of state gives the location of the wavefunction for each energy state. States very near the HOMO level are located primarily on the adenine bases. For any given state, the sum of the four residences add to unity.

with the most recently established dependence of electronic coupling between DNA bases in the stack on DNA conformational states: a diminution of the coupling between the DNA purine bases due to the pertinent conformational changes would 'arrest' the HOMO at one particular base. Whereas, conformationally induced increases in the above coupling ought to promote the 'HOMO trading' we revealed here. Our results are also in accordance with the analogous approach put forth most recently in Ref. [46] and in Ref. [88]. To be capable of formulating reasonable suggestions for experimentalists, we would need more detailed calculations not only on poly(dG)-poly(dC), but also on DNA with mixed base sequences.

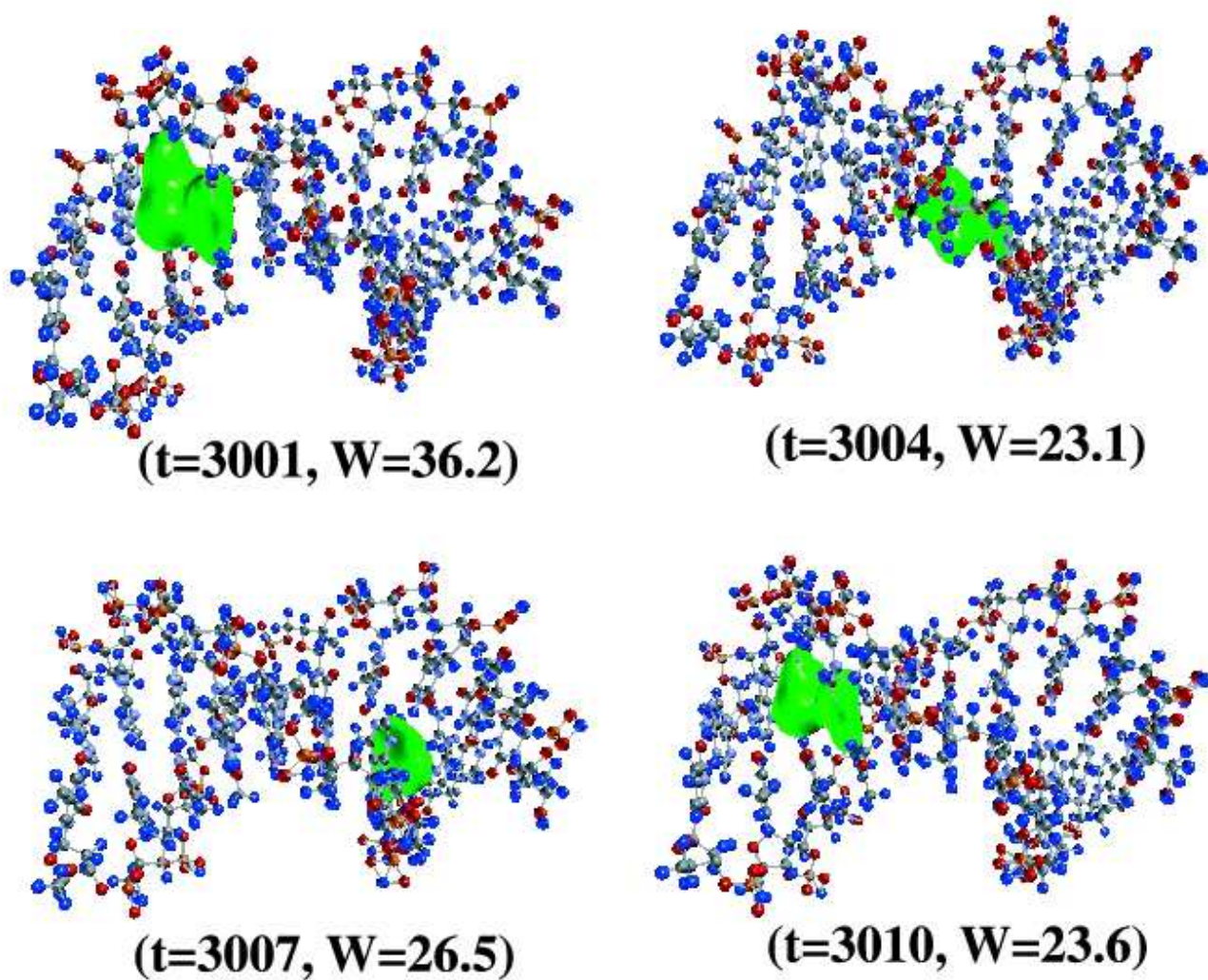


Fig. 7. Population density plots for the localised HOMO state as a function of time. The time between snapshots is 1.5 ps.

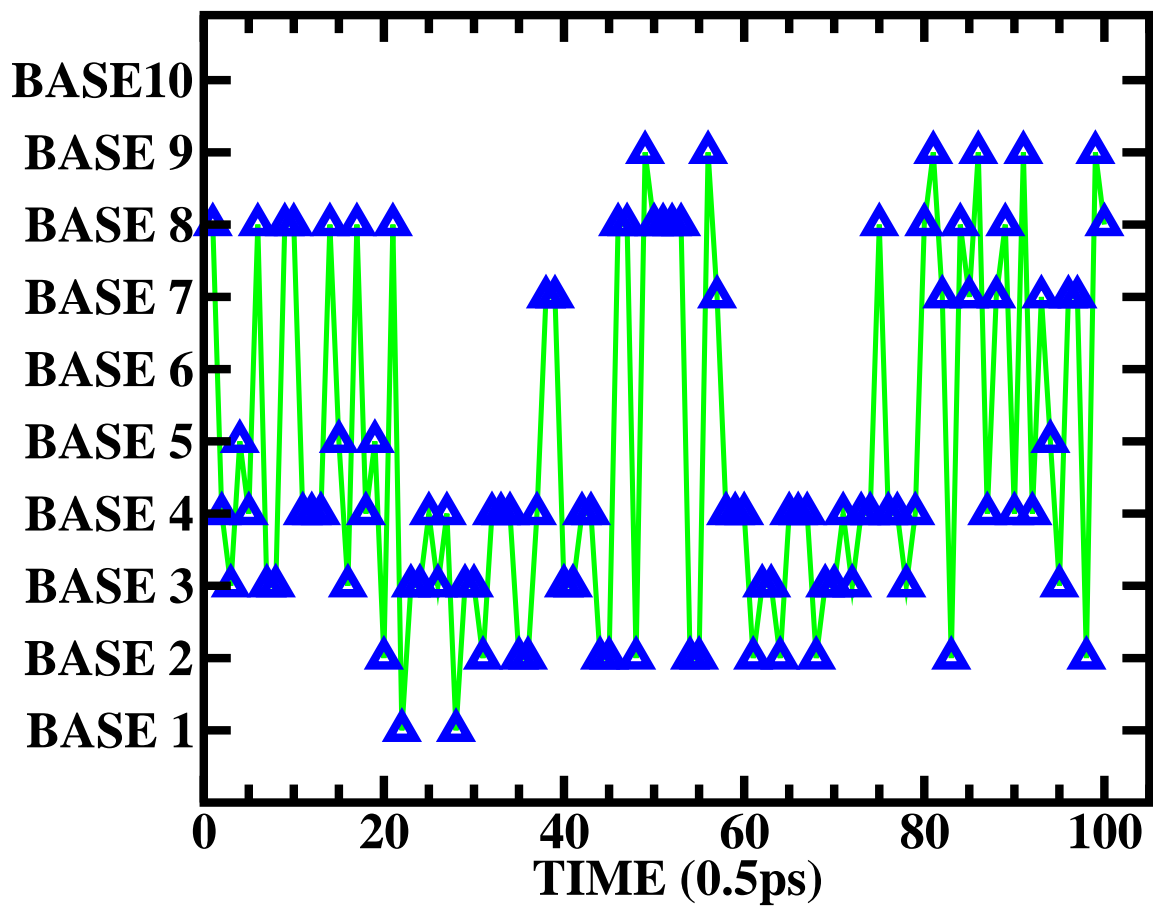


Fig. 8. Location of the HOMO as function of time. The ten bases are the ten adenine bases on one strand of the DNA. The HOMO is located only on adenine bases.

3. Effective tight-binding Hamiltonians for *long* DNA strands and complete sequences

In this section, we focus on whether DNA, when treated as a quantum wire in the fully coherent low-temperature regime, is conducting or not. To this end, we study and generalise a tight-binding model of DNA which has been shown to reproduce experimental [25] as well as *ab-initio* results [89]. A main feature of the model is the presence of sites which represent the sugar-phosphate backbone of DNA but along which no electron transport is permissible. We emphasize that the model is constructed to take into account the HOMO-LUMO gap observed in the DFT-based studies in chapter 2 as well as the observed absence of transport along the backbone. We measure the effectiveness of the electronic transport by the *localisation length* ξ , which roughly speaking parametrises whether an electron is confined to a certain region ξ of the DNA (insulating behaviour) or can proceed across the full length L ($\leq \xi$) of the DNA molecule (metallic behaviour).

3.1. The ladder model

A convenient tight binding model for DNA can be constructed as follows: it has two central conduction channels in which individual sites represent an individual base; these are interconnected and further linked to upper and lower sites, representing the backbone, but are *not* interconnected along the backbone. Every link between sites implies the presence of a hopping amplitude. The Hamiltonian H_L for this ladder-like model is given by

$$\begin{aligned}
 H_L = & \sum_{i=1}^L \sum_{\tau=1,2} (t_{i,\tau} |i, \tau\rangle \langle i+1, \tau| + \varepsilon_{i,\tau} |i, \tau\rangle \langle i, \tau|) \\
 & + \sum_{q=\uparrow,\downarrow} (t_i^q |i, \tau\rangle \langle i, q(\tau)| + \varepsilon_i^q |i, q\rangle \langle i, q|) \\
 & + \sum_{i=1}^L t_{1,2} |i, 1\rangle \langle i, 2|
 \end{aligned} \tag{2}$$

where $t_{i,\tau}$ is the hopping amplitude between sites along each branch $\tau = 1, 2$ and $\varepsilon_{i,\tau}$ is the corresponding onsite potential energy. t_i^q and ε_i^q give hopping amplitudes and onsite energies at the backbone sites. Also, $q(\tau) = \uparrow, \downarrow$ for $\tau = 1, 2$, respectively. The parameter t_{12} represents the hopping between the two central branches, i.e., perpendicular to the direction of conduction. Quantum chemical calculations with semi-empirical wave function bases using the SPARTAN package [90] results suggest that this value, dominated by the wave function overlap across the hydrogen bonds, is weak and so we choose

$t_{12} = 1/10$.² As we restrict our attention here to pure DNA, we also set $\varepsilon_{i,\tau} = 0$ for all i and τ . Note that in this way, the energy gap has been made to be symmetric about $E = 0$. Hence when comparing with the results in section 2, a constant shift according to the neglected ionisation potentials has to be added.

The model (2) clearly represents a dramatic simplification of DNA. Nevertheless, in Ref. [25] it had been shown that an even simpler model — in which base-pairs are combined into a single site — when applied to an artificial sequence of repeated GC base pairs, poly(dG)-poly(dC) DNA, reproduces experimental data current-voltage measurements when $t_i = 0.37eV$ and $t_i^q = 0.74eV$ are being used. This motivates the above parametrisation of $t_i^q = 2t_i$ and $t_{i,\tau} \equiv 1$ for hopping between like (GC/GC, AT/AT) pairs. Assuming that the wave function overlap between consecutive bases along the DNA strand is weaker between unlike and non-matching bases (AT/GC, TA/GC, etc.) we thus choose $1/2$. Furthermore, since the energetic differences in the adiabatic electron affinities of the bases are small [91], we choose $\varepsilon_i = 0$ for all i . Due to the non-connectedness of the backbone sites along the DNA strands, the model (2) can be further simplified to yield a model in which the backbone sites are incorporated into the electronic structure of the DNA. The effective ladder model reads as

$$\begin{aligned} \tilde{H}_L = & \sum_{i=1}^L t_{1,2} |i, 1\rangle \langle i, 2| + \sum_{\tau=1,2} t_{i,\tau} |i, \tau\rangle \langle i+1, \tau| \\ & + \left[\varepsilon_{i,\tau} - \frac{\left(t_i^{q(\tau)}\right)^2}{\varepsilon_i^{q(\tau)} - E} \right] |i, \tau\rangle \langle i, \tau| + h.c. \quad . \end{aligned} \quad (3)$$

Thus the backbone has been incorporated into an *energy-dependent* onsite potential on the main DNA sites. This effect is at the heart of the enhancement of localization lengths due to increasing binary backbone disorder reported previously [42].

3.2. The numerical approach to localisation in a Hamiltonian tight-binding model

There are several approaches suitable for studying the transport properties of the model (2) and these can be found in the literature on transport in solid state devices, or, perhaps more appropriately, quantum wires. Since the variation in the sequence of base pairs precludes a general solution, we will use two methods well-known from the theory of disordered systems [78].

²Simulations with larger $t_{12} \sim 1/2$ give qualitatively similar results.

The first method is the iterative transfer-matrix method (TMM) [92–96] which allows us in principle to determine the localisation length ξ of electronic states in systems with cross sections $M = 1$ [25] and 2 (ladder) and length $L \gg M$, where typically a few million sites are needed for L to achieve reasonable accuracy for ξ . However, in the present situation we are interested in finding ξ also for viral DNA strands of typically only a few ten thousand base-pair long sequences. Thus in order to restore the required precision, we have modified the conventional TMM and now perform the TMM on a system of fixed length L_0 . This modification has been previously used [97–99] and may be summarised as follows: After the usual forward calculation with a global transfer matrix \mathcal{T}_{L_0} , we add a backward calculation with transfer matrix $\mathcal{T}_{L_0}^b$. This forward-backward-multiplication procedure is repeated K times. The effective total number of TMM multiplications is $L = 2KL_0$ and the global transfer-matrix is $\tau_L = (\mathcal{T}_{L_0}^b \mathcal{T}_{L_0})^K$. It can be diagonalised as for the standard TMM with $K \rightarrow \infty$ to give $\tau_L^\dagger \tau_L \rightarrow \exp[\text{diag}(4KL_0/\xi_\tau)]$ with $\tau = 1$ or $\tau = 1, 2$ for fishbone and ladder model, respectively. The largest ξ_τ for all τ then corresponds to the localisation lengths of the electron on the DNA strand and will be measured in units of the DNA base-pair spacing (0.34 nm).

The second method that we will use is the recursive Green function approach pioneered by MacKinnon [100, 101]. It can be used to calculate the dc and ac conductivity tensors and the density of states (DOS) of a d -dimensional disordered system and has been adopted to calculate all kinetic linear-transport coefficients such as thermoelectric power, thermal conductivity, Peltier coefficient and Lorentz number [102].

The main advantage of both methods is that they work reliably (i) for short DNA strands ranging from 13 (DFT studies [103]) base pairs up to 30 base pairs length which are being used in the nanoscopic transport measurements [89] as well as (ii) for somewhat longer DNA sequences as modelled in the electron transfer results and (iii) even for complete DNA sequences which contain, e.g. for human chromosomes up to 245 million base pairs [104].

3.3. Long DNA sequences: λ -DNA, centromers and (super-)promoters

We shall use 2 naturally occurring long DNA sequences (“strings”). (i) λ -DNA [105] is DNA from the bacteriophage virus. It has a sequence of 48502 base pairs and is biologically very well characterised. Its ratio α of like to un-like base-pairs is $\alpha_\lambda = 0.949$. (ii) centromeric DNA for chromosome 2 of yeast has 813138 base pairs [106] and $\alpha_{\text{centro.}} = 0.955$. This DNA is also rich in AT bases and has a high rate of repetitions which should be favourable for electronic transport.

Another class of naturally existing DNA strands is provided by so-called pro-

moter sequences. We use a collection of 4986 is these which have been assembled from the TRANSFAC database and cover a range of organisms such as mouse, human, fly, and various viruses. Promoter sequences are biologically very interesting because they represent those places along a DNA string where polymerase enzymes bind and start the copying process that eventually leads to synthesis of proteins. On average, these promoters consist of approximately 17 base-pairs, much too short for a valid localization length analysis by TMM. Therefore, we concatenate them into a 86827 base-pair long *super-promoter* with $\alpha_{\text{super-p.}} = 0.921$. In order to obtain representative results, 100 such super-promoters have been constructed, representing different random arrangements of the promoters, and the results presented later will be averages. As usual, averages of ξ are computed by averaging the normally distributed $1/\xi$ values.

Occasionally, we show results for “scrambled” DNA. This is DNA with the same number of A, T, C, G bases, but with their order randomised. Clearly, such sequences contain the same set of electronic potentials and hopping variations, but would perform quite differently in a biological context. A comparison of their transport properties with those from the original sequence thus allows to measure how important the exact fidelity of a sequence is. On average, we find for these sequences $\alpha_{\lambda/S} = 0.899$, $\alpha_{\text{centro./S}} = 0.9951$ and $\alpha_{\text{super-p./S}} = 0.901$.

A convenient choice of artificial DNA strand is a simple, 100000 base-pair long *random* sequence of the four bases, random-ATGC DNA, which we construct with equal probability for all 4 bases ($\alpha_{\text{random}} = 0.901$). We shall also ‘promote’ these random DNA strings by inserting all 4086 promoter sequences at random positions in the random-ATGC DNA ($\alpha_{\text{random/P}} = 0.910$).

3.4. Results for localization lengths

We have computed the energy dependence of the localization lengths for all sequences of section 3.3. In addition, λ -DNA, centromeric DNA and the super-promoter DNA where also scrambled 100 times and the localization length of each resulting sequence measured and the appropriate average constructed. Also, we constructed 100 promoted random-ATGC DNA sequences. As shown previously [42], the energy dependence of ξ reflects the backbone-induced two-band structure. The obtained $\xi(E)$ values for the lower band are shown in Fig. 9. In the absence of any onsite-disorder, we find two prominent peaks separated by $t_{1,2}$ and $\xi(E) = \xi(-E)$. We also see that λ -DNA has roughly the same $\xi(E)$ dependence as random-ATGC-DNA. The super-promoter has larger ξ values compared to random-atcg- and λ -DNA. Most surprisingly, centromeric DNA — the longest investigated DNA sequence — has a much larger localization length than all other DNA sequences. The order of like-to-unlike pair-ratios is

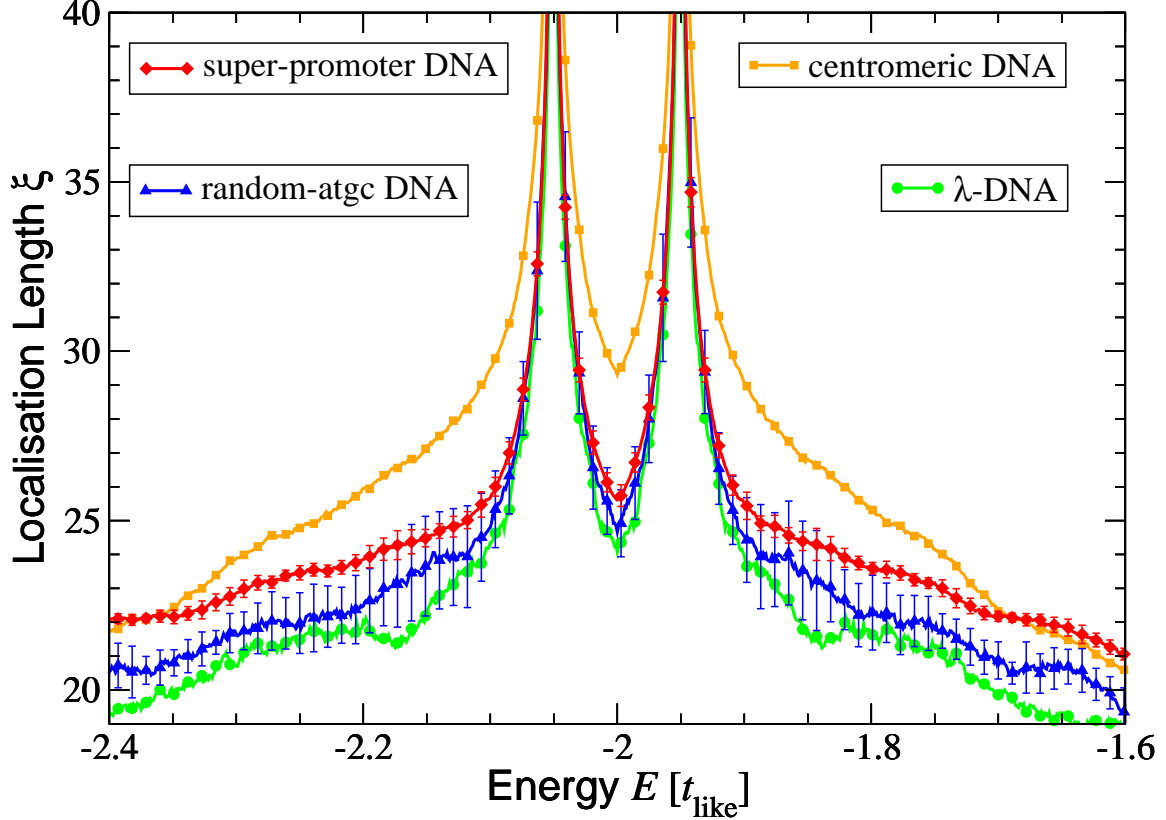


Fig. 9. Localization lengths ξ versus Fermi energy E for various clean DNA strands. Only every 10th symbol is shown. Error bars reflect the standard deviation after sampling the different sequences for random-ATGC and promoted DNA. The energy is measured in unit of hopping energy between like base pairs, i.e., $t_{\text{like}} = t_i = 0.37eV$.

$\alpha_{\text{centro.}} = 0.955 > \alpha_{\lambda} = 0.949 > \alpha_{\text{super-p.}} = 0.921 > \alpha_{\text{random}} = 0.901$ and one might expect that transport is favoured in sequences with large α . From Fig. 9, it is clear that this is not the case, λ -DNA has the smallest localization lengths, but the second largest α .

In Fig. 10, we add results for scrambled and promoted DNA. We find that promoting a given DNA sequence leads to small increases in localization length ξ for random DNA, whereas scrambling can lead to increase (centromeric and λ -DNA) as well as decrease (super-promoter). These results suggest that the promoters have a tendency towards larger localization lengths and thus enhanced transport.

3.5. Promoter sequences and E. coli binding sites

Let us now turn our attention to the transport properties of individual promoters rather than the artificially constructed super-promoters. Since their average lengths is 17 base-pairs and thus comparable to the localization lengths mea-

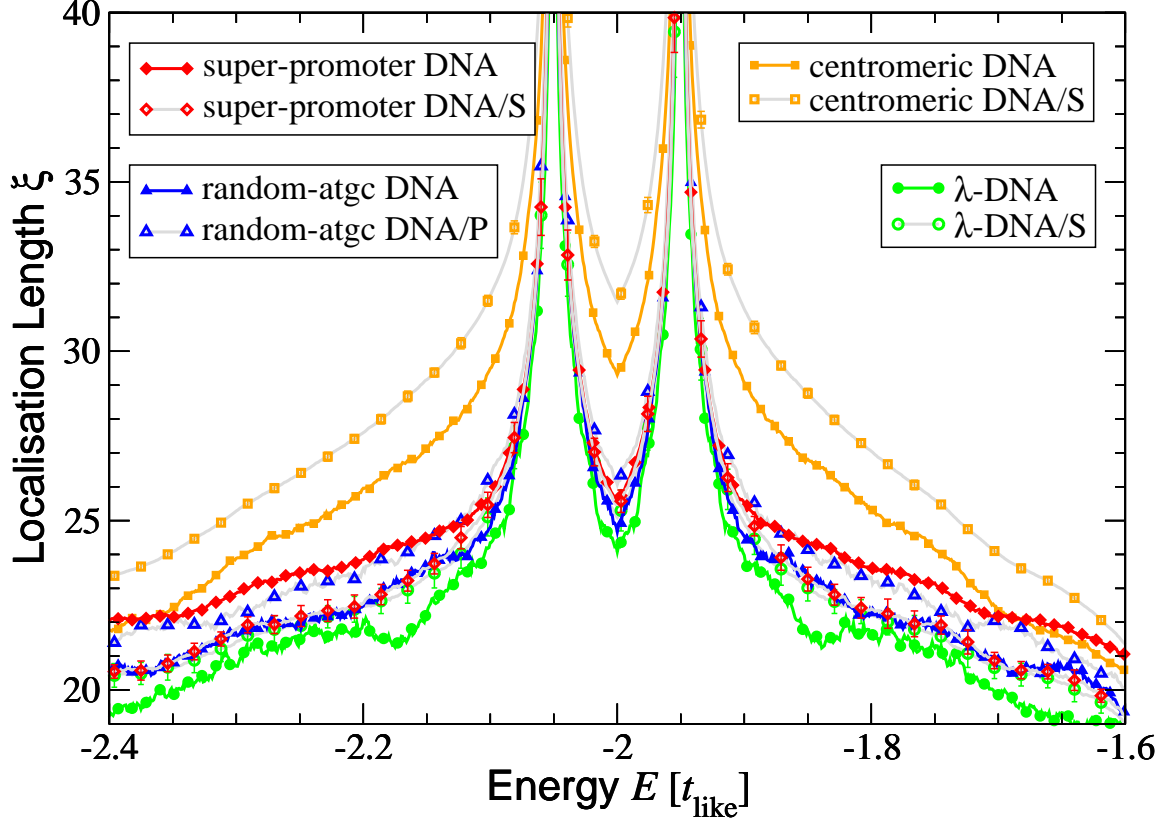


Fig. 10. Localization lengths ξ versus Fermi energy E for various clean DNA (solid symbols as in Fig. 9, error bars not shown for clarity), scrambled DNA (DNA/S, open \diamond , \square , \circ) and promoted DNA (DNA/R, open \triangle) strands. Only every 10th (20th) symbol is shown for clean (scrambled/promoted) DNA. Error bars reflect the standard deviation after sampling the different sequences for random-ATGC, scrambled and promoted DNA.

sured in the longer sequences, we can no longer use the TMM, but need to employ the RGFm mentioned in Section 3.2. While this method is capable of computing all thermoelectric transport coefficients, we shall restrict ourselves to presenting results for the conductance here.

In Fig. 11, we show results for averaged conductance in the upper band; both arithmetic and typical conductance have been calculated. We first note that the double-peak structure of Fig. 9 has vanished and only a single peak remains. This is because our results have been computed with perfectly-conducting leads attached to both ends of the DNA strands. This is close to the experimental situation, but the purely off-diagonal disorder in the DNA model is now masked by the ordered leads. Next, we observe that the promoters and their scrambled copies have larger conductances than random- and λ -promoters. λ -promoters has been constructed by cutting sequences with the same lengths as the true promoters out of λ -DNA at randomly selected positions along the DNA. Since

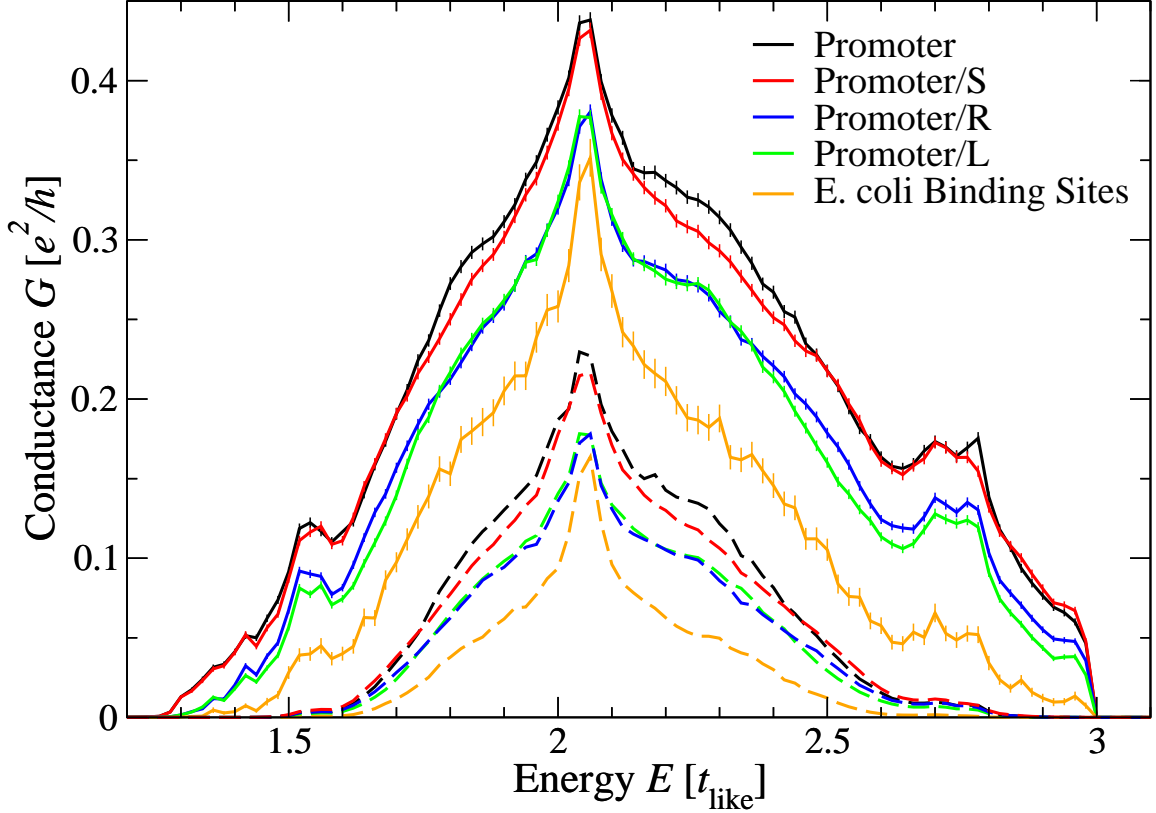


Fig. 11. Energy dependence of the conductance G for promoters, scrambled promoters (/S), random promoters (/R) and λ -promoters (/L). Solid lines denote the arithmetic, dashed lines the typical average of G . The error bars denote standard deviation obtained from the 4986 different promoters considered in each category (original and /S, /R, /L). These are not repeated for the typical averages for clarity.

α for random and λ -DNA is different, this allows us to check whether it is the order of base pairs or the value of α which dominated the value of G . Since $\alpha_{\text{promoter}} = 0.928 < \alpha_{\lambda} = 0.955$, but $G_{\text{promoter}} > G_{\lambda}$, it appears that as before the transport properties are not simply large if α is large. This suggests that it is indeed the fidelity of the sequence which is also important.

Typical and arithmetic averages share similar characteristics when comparing different sequences as shown in Fig. 11. However, the typical values are systematically smaller than their arithmetic counterparts. We therefore expect the distributions to be highly non-Gaussian and in Fig. 12 we see that this is indeed the case. We first note that both the original promoter as well as their scrambled version (/S) appear to have a slightly larger weight at $G > 0.05$ whereas both random and λ -DNA are peaked at $G \sim 0.025$. In addition, we find that there is a peak in the conductance distribution $P(G)$ at $G \sim 0.26$. This peak is most pronounced for the original promoter and their scrambled cousins, but much

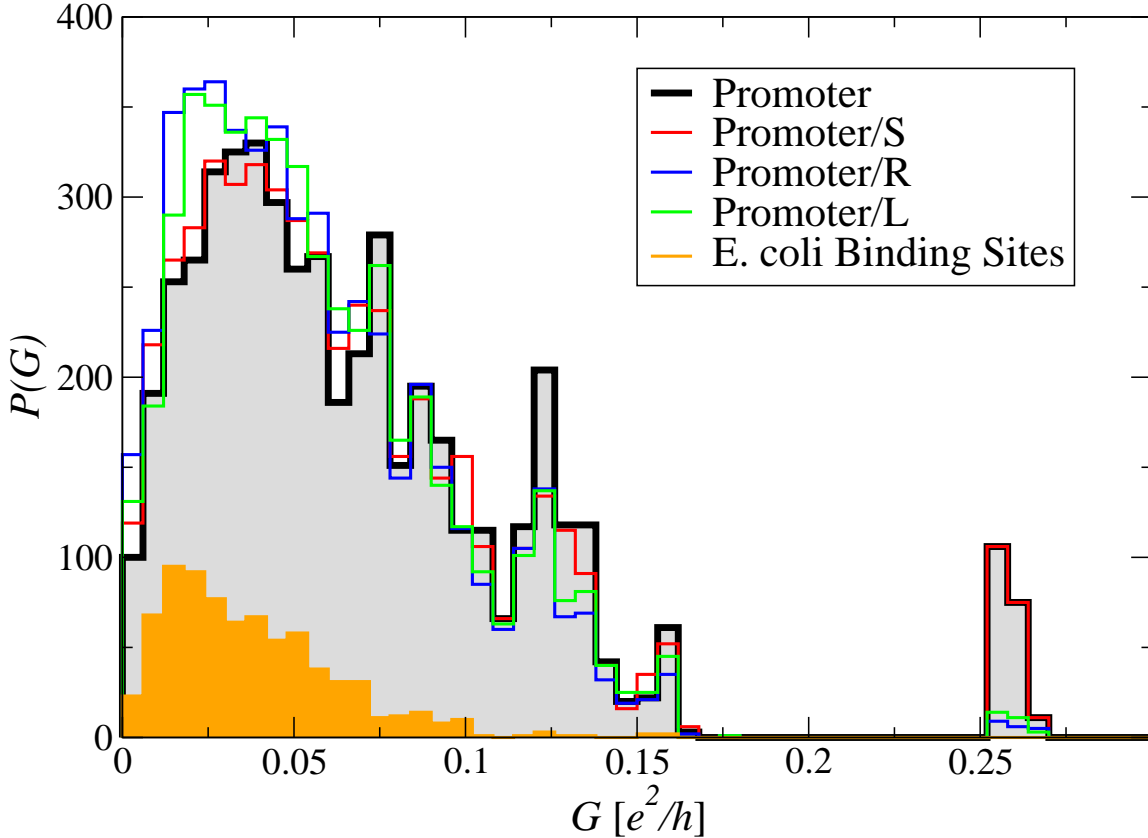


Fig. 12. Distribution function $P(G)$ for the conductances averaged over the energy range $[-5, 5]$. Only promoter and E. coli results have been shaded.

smaller for the artificial random- and λ -promoter.

In Figs. 11 and 12, we have also included results for computationally inferred 802 E. coli bindings sites [107]. Sequence-specific DNA-binding proteins perform a variety of roles in the cell, including transcriptional regulation. Our results show that the total conductance of these sequences is smaller than for promoters. However, their average length is ~ 25 so that the average *conductivity* is in fact larger when compared to promoters. This might be important in a biological context where one could envisage proteins to identify their binding sites differences on local conductivities.

4. Summary

The results presented in this chapter are preliminary results but indicate a marked difference in the nature of the electronic HOMO-LUMO states for the periodic and aperiodic structures of duplex DNA. These results indicate that the HOMO-LUMO states for the periodic structure are quite extended as would be expected for Bloch-like states while the HOMO-LUMO states for the aperiodic

structure demonstrates more localization. The concept of static localization in short DNA has previously been considered by Ladik [58, 59], and our results show that such a localization in our structure for aperiodic poly(dA)-poly(dT) DNA reaches far deeper in energy than just the band tail states. The localization phenomenon observed in the DNA double helix is the so-called Anderson localization which attributes to the *off-diagonal* disorder. This disorder results from dynamical variations in DNA intramolecular interactions and coupling of DNA with its environment. Turning our attention to longer DNA sequences, we next used this insight by modelling DNA as an off-diagonally disordered Anderson chain. However, in addition and contradistinction to previous studies using Anderson-type models, we include the sugar-phosphate backbone explicitly and by doing so retain the essential semi-conducting structure as observed in some experiments. Our results for the localization lengths suggest extended states even in non-periodic DNA up to ~ 20 base-pairs distances. This is roughly consistent with the previous results. Next, we study how transport properties differ between sequences and find that promoter sequences seem to have a tendency towards larger localization length, i.e. enhanced transport. This might point towards the importance of an electronic mechanism in the initial stages of DNA polymerase. Our results warrant further investigation, as the role of the dynamical localization and the sequence dependence may very well suggest an important mechanism of charge transport along the DNA molecule.

Acknowledgements

RAR gratefully acknowledges discussions with A. Rodriguez and M.S. Turner. JPL acknowledges discussions with D. Drabold, O. F. Sankey and T. Cheatham who prepared MD simulations. While the chapter has been prepared jointly, calculations in Sec. 2 were done by J. P. Lewis, H. Wang and R. Marsh, whereas Sec. 3 is based on results of R. A. Römer.

REFERENCES

1. Longe-Range Charge Transfer in DNA I, Topics in Current Chemistry Vol. **236**, edited by G. B. Schuster (Springer-Verlag, Heidelberg, 2004).
2. Longe-Range Charge Transfer in DNA II, Topics in Current Chemistry Vol. **237**, edited by G. B. Schuster (Springer-Verlag, Heidelberg, 2004).
3. R. G. Endres, D. L. Cox and R. R. P. Singh, Rev. Mod. Phys. **76**, 195 (2004).
4. D. Porath, G. Cuniberti, and R. Di Felice, Topics in Current Chemistry **237**, 183 (2004).
5. J. D. Watson and F. H. C. Crick, Nature **171**, 737 (1953).
6. D. D. Eley and D. I. Spivey, Trans. Faraday Soc. **58**, 411 (1962).
7. S. O. Kelley and J. K. Barton, Science **283**, 375 (1999).
8. B. Giese, S. Wessely, M. Spormann, U. Lindemann, E. Meggers, and M. E. Michel-Beyerle, Angew. Chem. Int. Ed. **38**, 996 (1999).

9. P. T. Henderson, D. Jones, G. Hampkian, Y. Kan, and G. B. Schuster, Proc. Natl. Acad. Sci. USA **96**, 8353 (1999).
10. C. Wan, T. Fiebig, S. O. Kelley, C. R. Treadway, J. K. Barton, and A. H. Zewail, Proc. Natl. Acad. Sci. USA **96**, 6014 (1999).
11. E. Meggers, M. E. Michel-Beyerle, and B. Giese, J. Am. Chem. Soc. **120**, 12950 (1998).
12. E. Meggers, D. Kusch, M. Spichty, U. Wille, and B. Giese, Angew. Chem. Int. Ed. **37**, 460 (1998).
13. K. Fukui and K. Tanaka, Angew. Chem. Int. Ed. **37**, 158 (1998).
14. F. D. Lewis, T. Wu, Y. Zhang, R. L. Letsinger, S. R. Greenfield, and M. R. Wasielewski, Science **277**, 673 (1997).
15. A. M. Brun and A. Harriman, J. Am. Chem. Soc. **116**, 10383 (1994); *ibid*, **114**, 3656 (1992).
16. Y. A. Berlin, A. L. Burin, and M. A. Ratner, J. Am. Chem. Soc. **123**, 260 (2001) and references therein.
17. R. N. Barnett, C. L. Cleveland, A. Joy, A. U. Landman, and G. B. Schuster, Science **294**, 567 (2001).
18. J. Jortner, M. Bixon, T. Langenbacher, and M. Michel-Beyerle, Proc. Natl. Acad. Sci. USA **95**, 12759 (1998).
19. D. N. Beratan, S. Priyadarshy, and S. Risser, Chem. Biol. **4**, 3 (1997).
20. S. Priyadarshy, S. M. Risser, and D. N. Beratan, J. Phys. Chem. **100**, 17678 (1996).
21. Ch. Adessi, S. Walch, and M. P. Anantram, Phys. Rev. **B67**, 081405 (2003).
22. F. C. Grozema, L.D.A. Siebbeles, Yu.A. Berlin, and M. A. Ratner, Chem. Phys. Chem. **6**, 536 (2002).
23. P. de Pablo, F. Moreno-Herrero, J. Colchero, J. GomezHerrero, P. Herrero, A. M. Baro, P. Ordejon, J. M. Soler, and E. Artacho, Phys. Rev. Lett. **85**, 4992 (2000).
24. P. Maragakis, R. L. Barnett, E. Kaxiras, M. Elstner, and T. Frauenheim, Phys. Rev. **B66**, 241104 (2002).
25. G. Cuniberti, L. Craco, D. Porath, and C. Dekker, Phys. Rev. **B 65**, 241314 (2002).
26. J. Reynisson and S. Steenken, Phys. Chem. Chem. Phys. **4**, 527 (2002).
27. H. Sugiyama and I. Saito, J. Am. Chem. Soc. **118**, 7063 (1996).
28. Y. Yoshioka et al., J. Am. Chem. Soc. **121**, 8712 (1999).
29. H. Wang and J. P. Lewis, Phys. Rev. Lett. **93**, 016401 (2004).
30. J. P. Lewis, T. E. Cheatham, E. B. Starikov, H. Wang, and O. F. Sankey, J. Phys. Chem. **B107**, 2581 (2003).
31. S. Roche, Phys. Rev. Lett. **91**, 108101 (2003).
32. S. Roche, D. Bicout, E. Maciá, and E. Kats, Phys. Rev. Lett. **91**, 228101 (2003).
33. K. Iguchi, Int. J. Mod. Phys. **B 17**, 2565 (2003).
34. S. Roche and E. Maciá, Mod. Phys. Lett. **B 18**, 847 (2004).
35. H. Yamada, E. B. Starikov, D. Hennig, and J. F. R. Archilla, Eur. Phys. J. **E 17**, 149 (2005).
36. H. Yamada, Phys. Lett. **A** (2004).
37. H. Yamada, Int. J. Mod. Phys. **B 18**, 1697 (2004).
38. K. Iguchi, Int. J. Mod. Phys. **B 18**, 1845 (2004).
39. C.-T. Shih, phys. stat. sol. (b) (2005), submitted.
40. C.-T. Shih, Phys. Rev. Lett. (2005), submitted.
41. D. K. Klotsa, R. A. Römer, and M. S. Turner, In Proceedings 27th International Conference on the Physics of Semiconductors(Q5 129), Flagstaff, Arizona 328 (2004).
42. D. K. Klotsa, R. A. Römer, and M. S. Turner, Biophys. J. **89**, 2187 (2005).
43. R. Bruinsma, G. Gruer, M. R. D'Orsogna, and J. Rudnik, Phys. Rev. Lett. **85**, 4393 (2000).
44. G. Brunaud, F. Castet, A. Fritsch, and L. Ducasse, Phys. Chem. Chem. Phys. **5**, 2104 (2003).

45. I. V. Kurnikov, G. S. M. Tong, M. Madrid, and D. Beratan, *J. Phys. Chem. B* **106**, 7 (2002).
46. A. A. Voityuk, K. Siriwong, and N. Rosch, *Phys. Chem. Chem. Phys.* **3**, 5421 (2001).
47. E. B. Starikov, *Phil. Mag.* **85**, 3435 (2005).
48. D. Henning, E. B. Starikov, J. F. R. Archilla, and F. Palmero, *J. Bio. Phys.* **30**, 227 (2004).
49. E. B. Starikov, *J. Photochem. Photobio. C* **3**, 147 (2002).
50. E. B. Starikov, *Phys. Chem. Chem. Phys.* **4**, 4523 (2002).
51. E. B. Starikov, *Mod. Phys. Lett. B* **18**, 825 (2004).
52. T. Tanabe, K. Noda, M. Saito, E. B. Starikov, and M. Tateno, *Phys. Rev. Lett.* **93**, 043201 (2004).
53. J. Cuevas, E. B. Starikov, J. F. R. Archilla, and D. Henning, *Mod. Phys. Lett. B* **18**, 1319 (2004).
54. P. W. Anderson, *Phys. Rev.* **109**, 1492 (1958).
55. J. Dong and D. A. Drabold, *Phys. Rev. Lett.* **80**, 1928 (1998).
56. P. Thomas and H. Overhof, Dordrecht (Kluwer Academic Publisher, 2001).
57. W. Gotze, *Philos. Mag.* **B43**, 219 (1981).
58. J. Ladik, M. Seel, P. Otto, and A. K. Bakhshi, *Chem. Phys.* **108**, 203 (1986).
59. Y.-J. Ye, R. S. Chen, J. Shun, and J. Ladik, *Solid State Commun.* **119**, 175 (2001).
60. S. Arnott, and D. W. Hukins, *Biochem. Biophys. Res. Comm.* **47**, 1504 (1972).
61. D. A. Pearlman, D. A. Case, J. W. Caldwell, W. S. Ross, T. E. Cheatham, S. Debolt, D. Ferguson, G. Seibel, and P. Kollman, *Comput. Phys. Comm.* **91**, 1 (1995).
62. B. R. Brooks, R. E. Brucoleri, B. D. Olafson, D. J. States, S. Swaminathan, and M. J. Karplus, *Computat. Chem.* **4**, 187 (1983).
63. J. Aqvist, *J. Phys. Chem.*, **94**, 8021 (1990).
64. W. D. Cornell, P. Cieplak, C. I. Bayly, I. R. Gould, K. M. Merz, D. M. Ferguson, D. C. Spellmayer, T. Fox, J. W. Caldwell, and P. A. Kollman, *J. Am. Chem. Soc.* **117**, 5179 (1995).
65. D. R. J. Langley, *Biomol. Struct. Dyn.*, **16**, 487 (1998).
66. W. G. Hoover, *Phys. Rev. A* **31**, 1695 (1985).
67. S. E. Feller, Y. Zhang, W. Pastor, and B. R. Brooks, *J. Chem. Phys.* **103**, 4613 (1995).
68. J. P. Ryckaert, G. Ciccotti, and H. J. C. Berendsen, *Comput. Phys.* **23**, 327 (1977).
69. U. Essmann, L. Perera, M. L. Berkowitz, T. Darden, H. Lee, and L. G. Pedersen, *J. Chem. Phys.* **103**, 8577 (1995).
70. D. L. Beveridge and K. J. McConnell, *Curr. Opin. Struct. Biol.* **10**, 182 (2000).
71. T. E. Cheatham and P. A. Kollman, *Annu. Rev. Phys. Chem.* **51**, 435 (2000).
72. T. E. Cheatham and M. A. Young, *Biopoly.* **56**, 232 (2001).
73. J. P. Lewis, K. R. Glaesemann, G. A. Voth, J. Fritsch, A. A. Demkov, J. Ortega, and O. F. Sankey, *Phys. Rev. B* **64**, 195103 (2001).
74. J. Harris, *Phys. Rev. B* **31**, 1770 (1985).
75. W. Foulkes and R. Haydock, *Phys. Rev. B* **39**, 12520 (1989).
76. A. A. Demkov, J. Ortega, O. F. Sankey, and M. P. Grumbach, *Phys. Rev. B* **52**, 1618 (1995).
77. O. F. Sankey and D. J. Niklewski, *Phys. Rev. B* **40**, 3979 (1989).
78. R. A. Römer and M. Schreiber, in *The Anderson Transition and its Ramifications — Localisation, Quantum Interference, and Interactions*, edited by T. Brandes and S. Kettmann (Springer, Berlin, 2003), Chap. Numerical investigations of scaling at the Anderson transition, pp. 3–19.
79. P. Biswas, P. Cain, R. A. Römer, and M. Schreiber, *phys. stat. sol. (b)* **218**, 205 (2000), ArXiv: cond-mat/0001315.
80. U. Dornberger, M. Leijon, and H. Fritzsche, *J. Biol. Chem.* **274**, 6957 (1999).

81. W. K. Olson, A. A. Gorin, X. J. Lu, and L. M. Hock, Proc. Natl. Acad. Sci. U.S.A. **95**, 11163 (1998).
82. H. Hellmann, Einführung in die Quantumchemie, Franz Duetsche, Leipzig 1937.
83. R.P. Feynman, Phys. Rev. **56**, 340 (1939).
84. R. A. Römer and P. Ziesche, J. Phys. A: Math. Gen. **34**, 1485 (2001).
85. M. Preuss, W. G. Schmidt, K. Seino, J. Furthmuller, and F. Bechstedt, J. Comput. Chem. **25**, 112 (2003).
86. S.D. Wetmore, R.J. Boyd, and L.A. Eriksson, Chem. Phys. Lett. **322**, 129 (2000).
87. V.M. Orlov, A.N. Smirnow, and Y. Varshavsky, Tetrahedron **48**, 4377 (1976).
88. A. Troisi and G. Orlandi, J. Phys. Chem. B **106**, 2093 (2002).
89. O. R. Davies and J. E. Inglesfield, Phys. Rev. B **69**, 195110 (2004).
90. SPARTAN version 5.0, User's Guide, Wavefunction Inc., 18401 Von Karman Ave., Suite 370 Irvine, CA 92612.
91. S. S. Wesolowski, M. L. Leininger, P. N. Pentchev, and H. F. Schaefer III, J. Am. Chem. Soc. **123**, 4023 (2001).
92. J.-L. Pichard and G. Sarma, J. Phys. C **14**, L127 (1981).
93. J.-L. Pichard and G. Sarma, J. Phys. C **14**, L617 (1981).
94. A. MacKinnon and B. Kramer, Z. Phys. B **53**, 1 (1983).
95. B. Kramer and A. MacKinnon, Rep. Prog. Phys. **56**, 1469 (1993).
96. A. MacKinnon, J. Phys.: Condens. Matter **6**, 2511 (1994).
97. K. Frahm, A. Müller-Groeling, J. L. Pichard, and D. Weinmann, Europhys. Lett. **31**, 169 (1995).
98. R. A. Römer and M. Schreiber, Phys. Rev. Lett. **78**, 4890 (1997).
99. M. L. Ndawana, R. A. Römer, and M. Schreiber, Europhys. Lett. **68**, 678 (2004).
100. A. MacKinnon, J. Phys.: Condens. Matter **13**, L1031 (1980).
101. A. MacKinnon, Z. Phys. B **59**, 385 (1985).
102. R. A. Römer, C. Villagonzalo, and A. MacKinnon, J. Phys. Soc. Japan **72**, 167 (2002), suppl. A.
103. P. J. Pablo, F. Moreno-Herrero, J. Colchero, J. Gomez Herrero, P. Hererro, P. Baro, A. M. an Ordejon, J. M. Soler, and E. Artacho, Phys. Rev. Lett. **85**, 4992 (2000).
104. B. Alberts, D. Bray, J. Lewis, M. Raff, K. Roberts, and J. Watson, *Molecular Biology of the Cell* (Garland, New York, 1994).
105. Bacteriophage lambda, complete genome [gi | 9626243 | ref | NC_001416.1 | [9626243]], Genbank Accession number NC_001416, <http://www.ncbi.nlm.nih.gov/entrez/>.
106. CEN2, Chromosome II centromere, <http://www.yeastgenome.org/>.
107. K. Robison, A. M. McGuire, and G. M. Church, Journal of Molecular Biology **284**, (1998).